Comparative Study of two Kalman Algorithms for Estimating the State of Charge of Lithium-Ion Cells at Ambient Temperature

Fuwu Yan [1,2], Chi Zhang [1,2], Changqing Du [1,2] [*] and Ching-Hsiang Cheng [1,2]

[1] Hubei Key Laboratory of Advanced Technology for Automotive Components (Wuhan University of Technology), Wuhan 430070, China;
[2] Hubei Collaborative Innovation Center for Automotive Components Technology, Wuhan 430070, China;
[*]E-mail: cq_du@whut.edu.cn

Kalman filters (KFs) are effective tools for estimating online state of charge (SOC), and a great variety of studies about different kinds of KFs have been published. However, problems remain in this field. First, the impact of ambient temperature on the internal parameters of equivalent circuit models (ECM) are seldom discussed. Second, comparative studies about different KFs are not fully validated under different conditions. To solve these problems, a modified equivalent circuit model was developed. The model was proposed to serve in ambient temperature and the usage of the total available capacity. Two typical nonlinear KFs, namely, the extended and unscented KFs were applied in SOC estimation. The model parameters were identified by hybrid pulse power characterization tests at 0, 15, 30, 45, and 55 °C. Meanwhile, the algorithms were validated under self-designed federal urban driving schedule sequence profiles at 0, 10, 20, 30, 40, and 50 °C with the same tuning setups. The robustness of the algorithm was also investigated in terms of voltage sensor uncertainty and the initial SOC offset. Results indicated that the proposed model can achieve the minimum mean absolute error and root mean squared error with the unscented KF at all test conditions.

1. INTRODUCTION

Currently, the urgency of using renewable energy in the face of serious environmental crisis urges us to use more of the clean energy sources. Hence, demand for rechargeable batteries for the storage of clean energy is experiencing a rapid growth. Rechargeable batteries play important roles in many applications, such as consumer electronics, power tools, portable power products, and electric vehicles (EVs). Among all kinds of rechargeable batteries, lithium-ion batteries have been attracting

special attention for EV applications owing to their high specific energy, low toxicity, and long cycle lifetime [1, 2].

The state of charge (SOC) indicates residual capacity and thus reflects the remaining driving range of an EV. Only an accurate SOC estimation can predict the correct remaining driving range, which is essential for easing the so-called "range anxiety" problems in EVs use. It can also determine the effective management strategy for preventing damages due to over-charging and over-discharging damages to rechargeable batteries. Therefore, it is considered as one of the most important battery control and monitoring parameters that must be obtained from a battery management system (BMS) [3]. However, given the complexity of the chemical and physical processes involved, the characteristics of batteries are more difficult to predict than the behaviors of other electric and mechanical devices. First, SOC is the inner state of a battery and cannot be measured directly. Second, several external characteristics, such as the hysteresis phenomena between charge and discharge, the flat slope of the open circle voltage (OCV) over the SOC curves, and the measurement noise, make SOC estimation increasingly challenging.

In recent years, extensive methods have been proposed for improving the accuracy of SOC estimation. Among the methods, coulomb counting is the most widely used. In this method, SOC is calculated by integrating current over time, and thus simple and easy to implement in BMS. However, given that it is an open-loop method, it has several inherent drawbacks. It influences the accumulated error is sensitive to the initial SOC value. One of the methods for addressing these drawbacks is considering OCV or charging efficiencies, as suggested in [4]. The other methods, collectively known as machine learning-based methods, include neural network (NN), fuzzy logic, and support vector machine (SVM). Fotouhi [5] combined an adaptive neuro-fuzzy inference system with a fast system identification technique to estimate the SOC. Liu [6] proposed an improved artificial neural network (ANN) model, which has a new training set and a voltage correction algorithm, to improve estimation accuracy. They were able to decrease root mean square error (RMSE) from 7.14% to 2.5% after training the ANN model by their new training set and sequentially decrease to 1.36% because of the voltage correction algorithm. Antón [7] set up an SVM SOC estimator for high-capacity lithium-iron manganese phosphate (LiFeMnPO$_4$) cells. The proposed model extracts model parameters from battery charging/discharging testing cycles; uses cell current, cell voltage, and cell temperature as independent variables; and can achieve an error of less than 6% over all ranges of operation. In summary, these methods do not require an intensive knowledge of battery systems, are universal methods that can be applied to all kinds' types of batteries, and can achieve good estimation accuracy if the training data match the loading conditions. However, a common drawback of the above methods is that model parameters are identified with offline data. Consequently, the estimation accuracy is only acceptable within narrow operating conditions in which they have been parameterized, and is relatively low in high dynamic loads. The robustness of these methods relies strongly on the quantity and quality of training data.

To overcome these issues, many efforts have been focused on closed-loop SOC observers, such as Kalman filter (KF) and its advanced modifications. KF is based on the minimum variance statistics of random state space theory, which was first proposed by R. E. Kalman in 1960. KF is an optimum state estimator for linear systems and thus rarely used in highly nonlinear lithium-ion battery systems. To

solve this problem, an extended Kalman filter (EKF) was developed by Plett in 2004 [8-10]. The core and foundation of the EKF is to linearize the system and measurement matrices by the first-order Taylor approximation of differential equations. Although its computational effort is heavier than those of conventional methods, it is acceptable for BMS. Bizeray [11] used the EKF algorithm with a thermal electrochemical model to estimate SOC. The model was constituted by partial-differential algebraic equations and discretized by Chebyshev orthogonal collocation for fast simulation. The results indicated that the estimation error can fall below 1% in specific cases. Fang [12] used the iterated EKF (ITEKF) with a single particle model to develop an adapted SOC algorithm. Through simulation and experimental verification, the proposed algorithm exhibited a good SOC estimation performance. Pérez [13] proposed an EKF estimator with the OCV model that considers the hysteresis influence. Sepasi [14, 15] improved the EKF algorithm by considering the battery aging phenomenon, and the SOC and voltage estimation errors do not exceed 1.5%. Wang [16] utilized the improved EKF (IEKF) with a one-order equivalent circuit model (ECM) to evaluate a battery pack's SOC, and the absolute maximum error was within 4.95%. Lee [17] considered the calculation time and proposed the EKF with a reduced-order ECM. The calculation time was remarkably reduced by model simplification and data rejection.

However, EKF also has several shortcomings. First, the EKF must calculate the Jacobian matrices, which are difficult to obtain in time-critical applications. Additionally, the EKF method may lead to cut-off errors and diverging results because he higher order derivatives of the Taylor approximation are ignored. To address the approximation issues, another approach, unscented Kalman filter (UKF), is developed. The UKF deals with the nonlinear propagation of the posterior mean and covariance by unscented transformation (UT). It can capture the posterior mean and covariance to the 3rd order accuracy, which the EKF cannot achieve [18]. In Refs. [19, 20], Plett discussed the theoretical advantages of UKF in detail. He [21, 22] utilized the UKF with the state-space model of coulomb counting and neural networks respectively. Both models can achieve an RMSE of less than 3.5% through federal urban driving schedule (FUDS) and dynamical stress testing (DST) validation. Tian [23] introduced the UKF to a modified ECM, considering the current rate and temperature. Then, the practical capacity of the battery was corrected by their modified model. With the proposal of various of KFs and their advanced modifications, some comparative studies have also been carried out to evaluate the algorithms in terms of estimation accuracy, robustness, and computational burden, such as in Refs. [24-29].

Nevertheless, several issues remain. First, the influence of ambient temperature on the ECM's internal parameters has been rarely discussed. Although temperature has been considered a critical external factor for lithium-ion batteries, most of the publications about ECMs have a certain limitation in estimation accuracy. According to the existing literature, ECM is either treated as a correction factor for recalibrating total capacity (e.g., Ref. [30],) or used for setting up a SOC-OCV-T look-up table, which improves the estimation accuracy at specific temperatures but has poor traceability for the dynamic performance because of the insufficient consideration of resistance-capacitance (RC) term. To the authors' best knowledge, this is the reason that the existing model usually achieves good accuracy in a stable environment but works poorly in real conditions, especially when the ambient temperature is uncertain. Xing [28] proposed an ECM that introduces temperature as a variable of internal resistance, but still does not consider the effect of the RC term. Second, in real-world EV or HEV applications,

batteries suffer from highly dynamic current loads and temperature changes. However, the comparative studies of different filters presented in the literature were usually validated under a certain condition.

In this light, a modified ECM was developed for the high-power commercial lithium-ion cells of EV applications. The proposed model considers the effect of ambient temperature and discharge rate. To estimate the SOC accurately, two KFs were implemented and compared. The algorithms were validated by a self-designed FUDS sequence profile at different temperatures. The remainder of this paper is organized as follows: The experimental procedures are introduced in Section 2. Four kinds of tests at different temperatures are described. The purpose of the static capacity and multiple-rate discharge tests is to recalibrate the temporary variations of the practical capacity caused by the temperature change and the dynamic current. The hybrid pulse power characterization (HPPC) and FUDS tests are utilized for parameters identification and algorithm validation, respectively. The model's mathematic description and validation are presented in Section 3. Followed by a brief introduction of Kalman theories and its implementation in online SOC estimation in Section 4. The experimental results and the comparison are presented in Section 5 to discuss the performance of the developed model and the two algorithms in terms of accuracy and robustness.

2. EXPERIMENTS

The experimental test bench, which consists of 1) 18650 cylindrical type of lithium-ion cells; 2) a programmable temperature chamber; 3) current, voltage, and temperature sampling cables; 4) a battery test station; 5) a host computer with BTS monitoring software; and 6) a Matlab R2017b for data processing, is shown in Fig. 1.
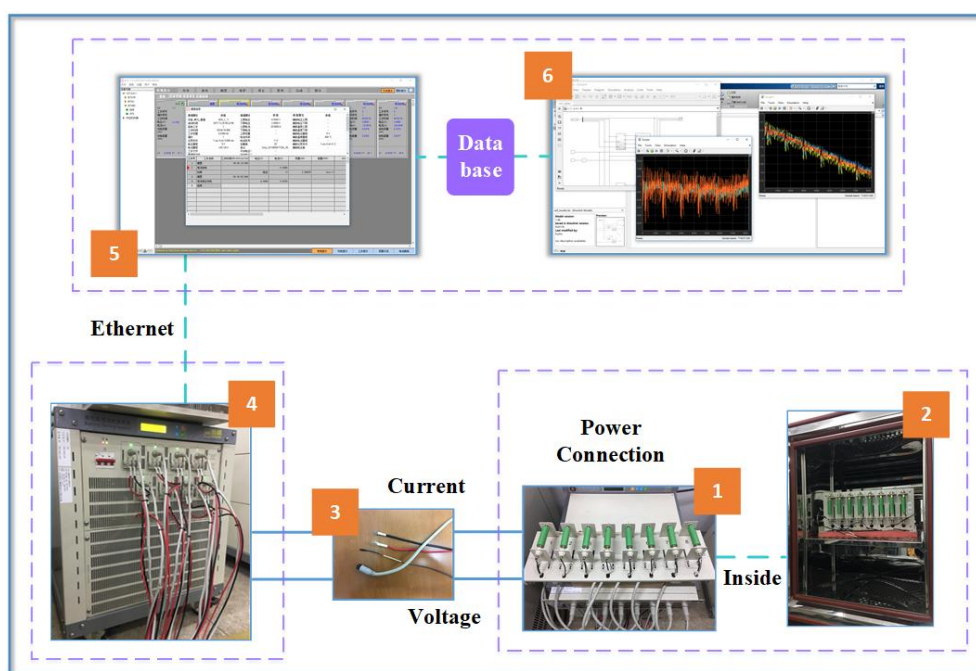

Figure 1. Schematic of the experimental testing bench.

The cells are of Sony US18650VTC5A type with a $LiNi_{1/3}Co_{1/3}Mn_{1/3}O_2$ cathode material, and the key specifications are shown in Table 1. This type is a high-specific-energy battery and designed for EVs. A temperature chamber with an adjustable temperature range of −40–100 °C is provided by a Chinese manufacturer (SUZHOU UNIQUE ENVIRONMENTAL TEST EQUIPMENT CO. LTD. China). It is responsible for the stable and controlled atmosphere temperature and humidity during the entire test. The NEWARER battery test station (NEWARE BTS-4002) is used for loading the cells according to the designed test procedure. The measured signals (incloud current, terminal voltage, and temperature) were collected by the sampling cables with errors less than 0.2%.

Table 1. Key specifications of the test cells.

Type	Nominal voltage	Nominal capacity	Upper cut-off voltage	Lower cut-off voltage	Maximum continuous discharge current
$Li(Ni_{1/3}Co_{1/3}Mn_{1/3})O_2$	3.6 V	2600 mAh	4.20 ±0.05 V	2.5 V	35 A

2.1. Static capacity test

Total available capacity is known to play an important role in SOC estimation and is sensitive to ambient temperature. A static capacity test was conducted at following temperatures: 0 °C, 15 °C, 30 °C, 45 °C, 55 °C. This test aims to calibrate the battery's available capacity and recalibrate the SOC under various temperatures. The test procedure at each temperature was as follows: 1) Charge the cells at a constant voltage of 4.20 V and a constant current of 1/3 C (0.833 A) (CC-CV method) until the cells reach the cut-off current of 0.04 C (0.1 A). 2) Rest the cells for 1 h to reach the equilibrium state. 3) Discharge the cells at 1/3 C constant current to the cut-off voltage of 2.5 V. The tests under each temperature were repeated three times, and the averag value was used as the available capacity.

2.2. Multiple-rate discharge test

The multiple-rate discharge test is a set of tests that discharge the cells at various current rates. The tests were also conducted at different temperatures (0 °C, 15 °C, 30 °C, 45 °C, and 55 °C). After resting at each temperature for at least 1 h, the cells were discharged by different constant currents of 0.2 C, 0.5 C, 1 C, 2 C, 5 C, and 8 C from the full-charged state to the lower cut-off voltage of 2.5 V. Finally, the cells were fully recharged to the upper cut-off voltage of 4.2 V by the CC-CV method.

2.3. Hybrid power pulse characterization test

For the identification of model parameters, an HPPC test was performed. The HPPC test profile is composed of a 30 s constant current discharge and a 10 s recharge with a 40 s interval [31]. After the

pulse sequence, the cell had a discharge of 5% depth of discharge (DOD) to the next SOC range and a resting period of 1 h before the sequence was repeated. We repeated this test 20 times to cover the DOD from 0% to 95%, then we used a 0.33 C current to traverse the SOC range. The pulse profile is shown in Fig. 2.
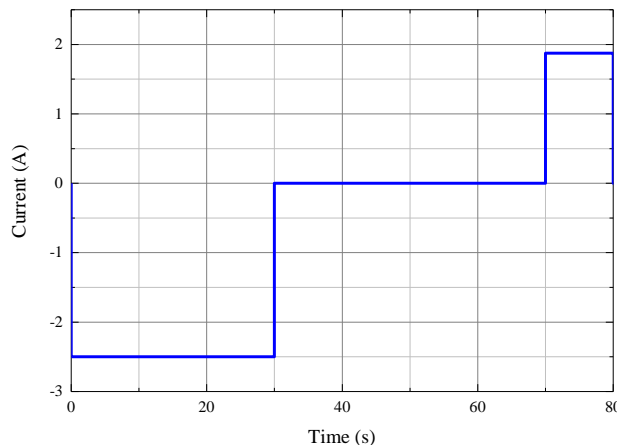

Figure 2. Hybrid Pulse Power Characterization (HPPC) Test Profile.

2.4. Federal urban driving schedule test

The FUDS test is often used for validating the SOC estimation algorithms for EV applications [32]. Thus an FUDS test was conducted. The test consisted of six typical FUDS sequences, and each sequence had a dynamic power load for 1372 s. Therefore, the total test lasted 8232 s. For the simulation of the actual battery SOC range in EVs and for the protection of the cells from overcharging, the initial SOC of the cell was set to 90% before the test.
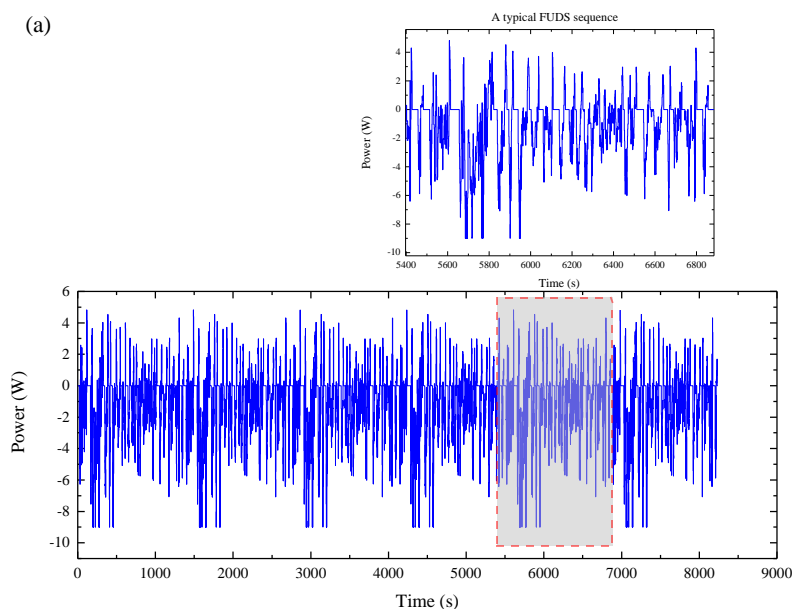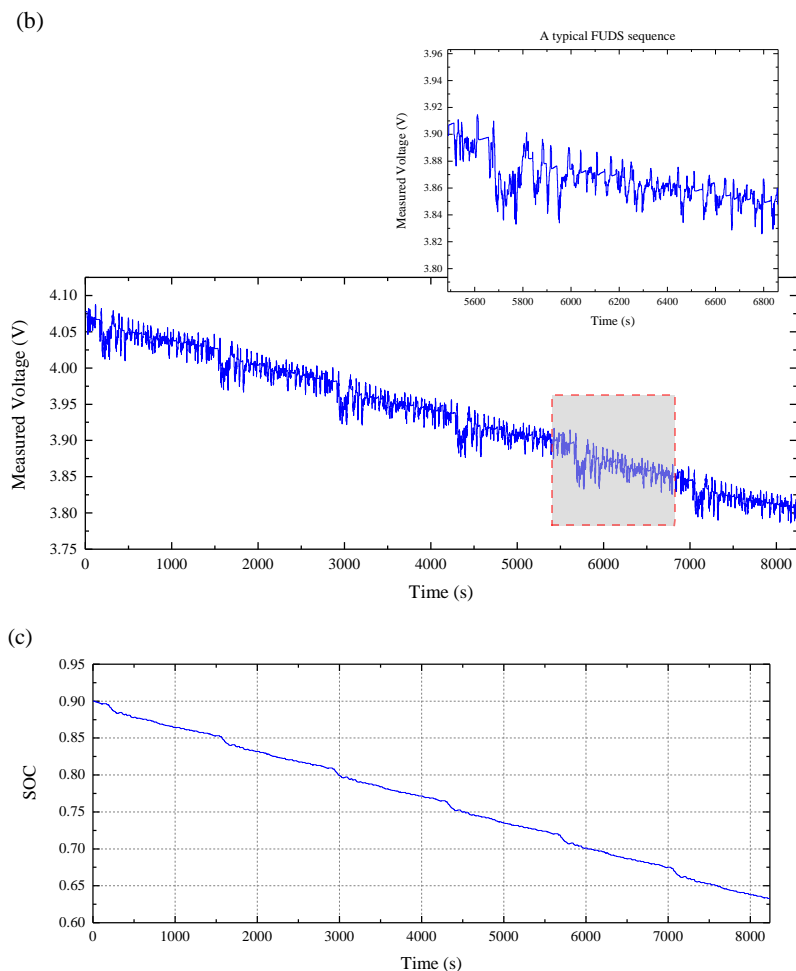
Figure 3. Power profile, measured voltage and SOC of VTC5A cells in FUDS testing dataset at 30 ℃.

The actual SOC was calculated by the accumulative Ampere-hours flowing in and out of the battery. The test was run from 0 °C to 50 °C with an interval of 10 °C. The completed power profile, measured voltage and the cumulative SOC at 30 °C are shown in Fig. 3 as examples.

3. DESCRIPTION OF CELL MODEL

For the accurate estimation of the SOC, a good battery state space model must be available. Various battery models have been studied for SOC estimation, such as electrochemical models [11, 33-35], black box models [24, 36-38], and ECMs [39, 30, 26, 17, 9, 32, 40]. A physics-based electrochemical model can capture the temporally evolved and spatially distributed behavior of the essential states of a battery [41]. It relies on the fundamental laws of transport, kinetics, and thermodynamics and requires the inputs of many physical parameters. Thus, it is the most accurate, yet most complex model. Black box models include NN-based models, fuzzy logic models, and SVMs. These models do not require a detailed knowledge of battery systems. Thus, they are universal methods that can be applied to all types of batteries and can achieve good accuracy if the training data match with

the loading conditions. However, a common drawback of black box methods is that the model parameters are identified with offline data. Consequently, the estimation accuracy is only acceptable within the narrow operating conditions in which they have been parameterized, but is relatively low in high dynamic loads. Moreover, the robustness of these methods strongly relies on the quantity and quality of training data. ECMs are the most common models associated with a KF in the estimation of the SOC. In ECM, the dynamic behavior of the battery is simulated by electrical elements including virtual voltage source, resistors, and capacitors. Twelve lumped ECM models have been discussed in the literature [26]. Accuracy can be improved by adding RC terms in the model, but the computational burden will increase in the process.

3.1. Model equations and description

To achieve a compromise between accuracy and complexity, we adopted the first-order RC network with a zero-state hysteresis model. The mathematical model can be expressed by:

$$U_l = U_{oc} + IR_0 + U_p \qquad (1)$$

$$\overline{U_p} = -\frac{1}{R_p C_p} U_p + \frac{1}{C_p} I \qquad (2)$$

Where U_l is the measured terminal voltage of the cell, and I is the main circuit current. The discharge current is negative while the charge current is positive. The OCV (U_{oc}), which is a nonlinear function of the SOC and ambient temperature. Ohm resistance is represented by R_0 and is dependent on the SOC and the current directions (charge or discharge). Polarization resistance and polarization capacitance are represented by R_p and C_p, respectively. They are connected in parallel to form a RC network, which represents the resistance and capacitance of the double-layer in the charge transfer processes [42]. Their values are calculated using the SOC-temperature 2-D look-up table. The schematic of the ECM is depicted in Fig. 4.
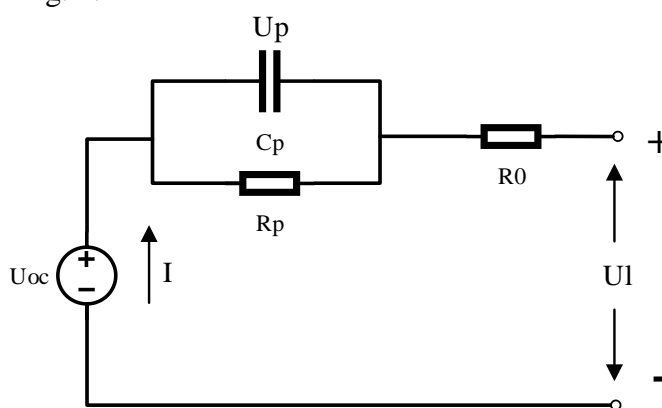

Figure 4. Schematic of the equivalent circuit model.

3.2. Model parameter identification of the cell

As mentioned in Section 2.3, the parameters of the proposed model were determined through the HPPC test. The voltage response of each hybrid current pulse was fitted by the least square method. The

hybrid current pulse covered the SOC from 5% to 100% with an interval of 5%, that is, 20 SOC points in total. Fig. 5 shows the identified results of the cells under test temperatures. Fig. 5 (a) exhibits the SOC–OCV correlation. Here the OCV was measured by the voltage value of the last 1 h rest between each SOC point. As shown in Figs. 5 (b) and (c), the Ohm resistance in both discharge and charge processes show a saddle shape with the middle low and the ends high. Meanwhile, resistance increased with decreasing temperature, and the increase became remarkable when the temperature was near 0 °C. Figs. 5 (d) and (e) show the polarization resistance and polarization capacitance. Similar to the Ohm resisitance, the polarization resistance and capacitance showed a high dependency on temperature. It is noted that the polarization resistance increased rapidly when the SOC droped from 25% to 5%, and remained stable from 25% to 65%.
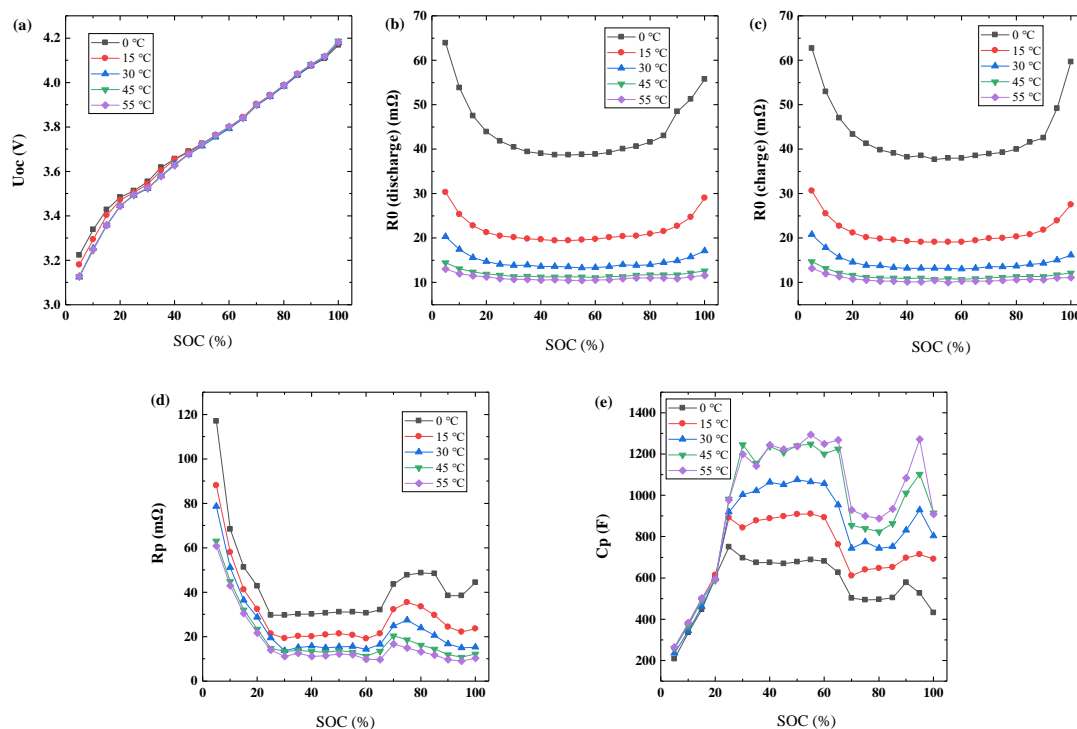

Figure 5. Identified parameters of the model at different temperatures.

3.3. Model validation and result

For the evaluation of model performance at different temperatures, the FUDS test described in Section 2.4 was performed on the cells. Here, we defined the parameters identified at 30 °C as the "conventional model". The simulation results of our proposed model and the conventional model were compared. Fig. 6 (a) exhibits the voltage response of the proposed model and the conventional first-order RC ECM. The data were obtained by the sampling or simulating a period of 1 sec. For readability, the completed FUDS cycle are shown in the enlarged window. Fig. 6 (b) illustrates the absolute error of the two comparative models at 0 °C. The proposed model, considering the temperature factor has a better tracking ablity than the conventional model. Meanwhile, the mean absolute error (MAE) and the RMSE are introduced to evaluate the accuracy quantitatively.
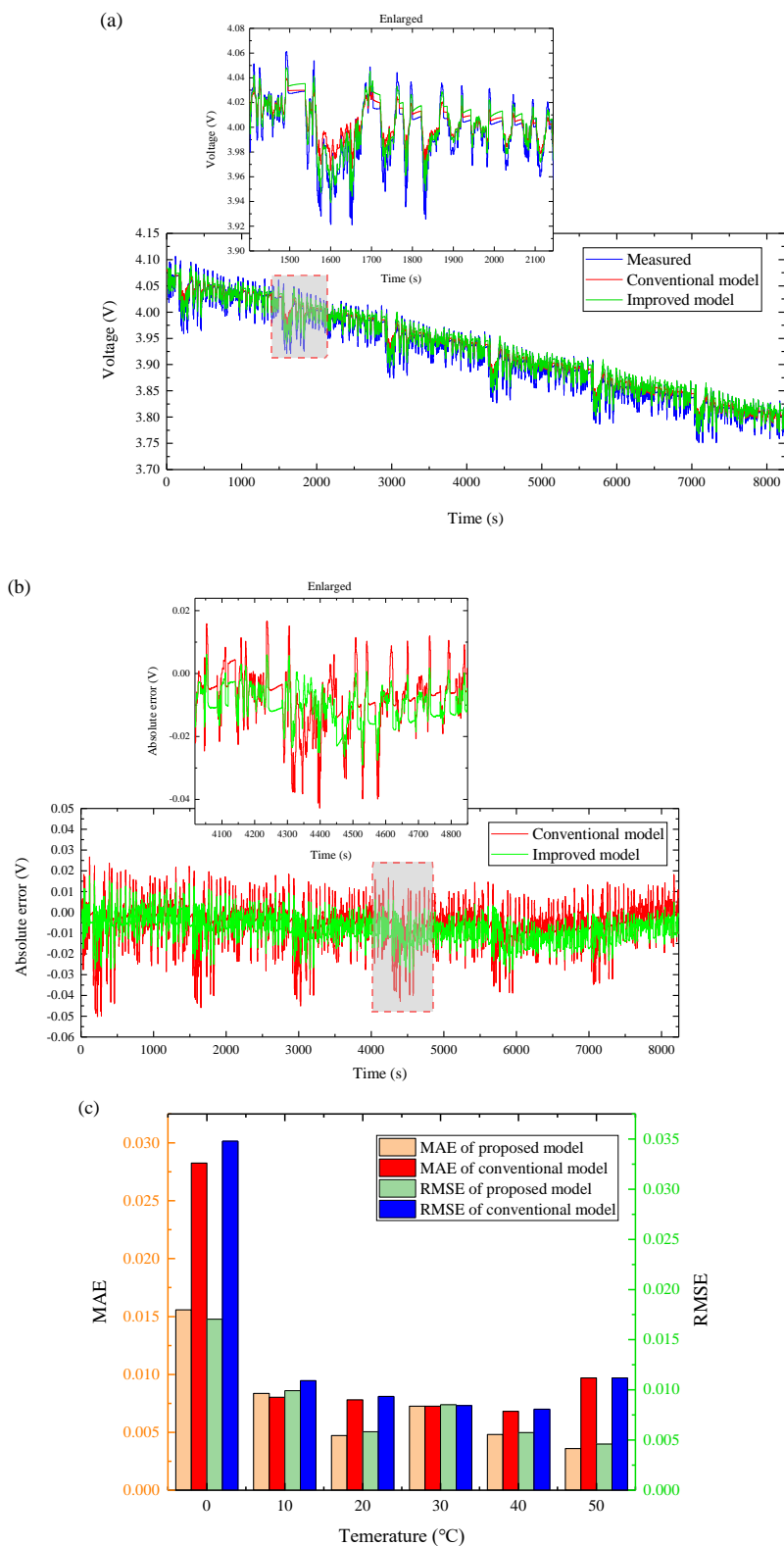
Figure 6. Results of the model voltage response. (a) Experimental and simulation voltage curves of the proposed model and origin model at 0 °C, (b) Enlarged window of a typical FUDS cycle, (c) MAE and RMSE of the proposed model and origin model at different temperatures.

The errors at different temperatures are shown in Fig. 6 (c). Obviously, both MAE and RMSE decreased at temperatures lower and higher than 30 °C. The RMSE of the proposed model is 1.705%,

whereas that of the the conventional model was 3.478%. The proposed model achieved an improvement of 50.9% in voltage tracking ability at 0 °C.

4. IMPLEMENTATION OF THE KALMAN FILTER

In this section, two kinds of KF algorithms, including EKF and UKF were applied in SOC estimation. The detailed procedure is described as follows.

4.1. Linear Kalman filter

Linear Kalman filter (LKF) is a mature algorithm that has been widely used for system state estimation and published by many papers. The theory is introduced briefly in this section.

The discretized state–space equation and the measurement equations can be described as follows:

$$x_{k+1} = A_k x_k + B_k u_k + \Gamma_k \omega_k \qquad (3)$$
$$y_k = C_k x_k + D_k u_k + v_k \qquad (4)$$

where $x_k \in R^n$ is the state vector of the considered n-dimension system at time index k. $u_k \in R^p$ is the deterministic input to the system; $y_k \in R^m$ is the measured quantity; and $A_k \in R^{n \times n}$, $B_k \in R^{n \times p}$, $C_k \in R^{m \times n}$, and $D_k \in R^{m \times p}$ are the matrices of transition, input, output, and feedforward, respectively. They work together to describe the dynamics of the system. Two random variables, ω_k and v_k, represent the process noise and measurement error, respectively. Both are assumed to be uncorrelated Gaussian distributed white noises. Their variance can be defined by equation (5) and (6).

$$E[\omega_n \omega_k^T] = \begin{cases} Q_k, & n = k \\ 0, & n \neq k \end{cases} \qquad (5)$$

$$E[v_n v_k^T] = \begin{cases} R_k, & n = k \\ 0, & n \neq k \end{cases} \qquad (6)$$

where Q_k is the variance matrix of the process, and R_k is the variance matrix of the measurement.

The algorithm is operated specifically by the following calculation sequences:

Initialization:
$$\hat{x}_{0|0} = E(x_0) \qquad (7)$$
$$P_{0|0} = E[(x_0 - \hat{x}_{0|0})(x_0 - \hat{x}_{0|0})^T] \qquad (8)$$

Prediction update:
$$\hat{x}_{k|k-1} = A_{k-1} \hat{x}_{k-1|k-1} + B_{k-1} u_{k-1} \qquad (9)$$
$$P_{k|k-1} = A_{k-1} P_{k-1|k-1} A_{k-1}^T + \Gamma_{k-1} Q_{k-1} \Gamma_{k-1}^T \qquad (10)$$

Kalman gain update:
$$K_k = P_{k|k-1} C_k^T (C_k P_{k|k-1} C_k^T + R_k)^{-1} \qquad (11)$$

Measurement update:
$$\hat{x}_{k|k} = \hat{x}_{k|k-1} + K_k(y_k - C_k \hat{x}_{k|k-1} - D_k u_{k-1}) \qquad (12)$$
$$P_{k|k} = (I - K_k C_k) P_{k|k-1} \qquad (13)$$

To be more intuitive, the working principle can be present as shown Fig. 7.
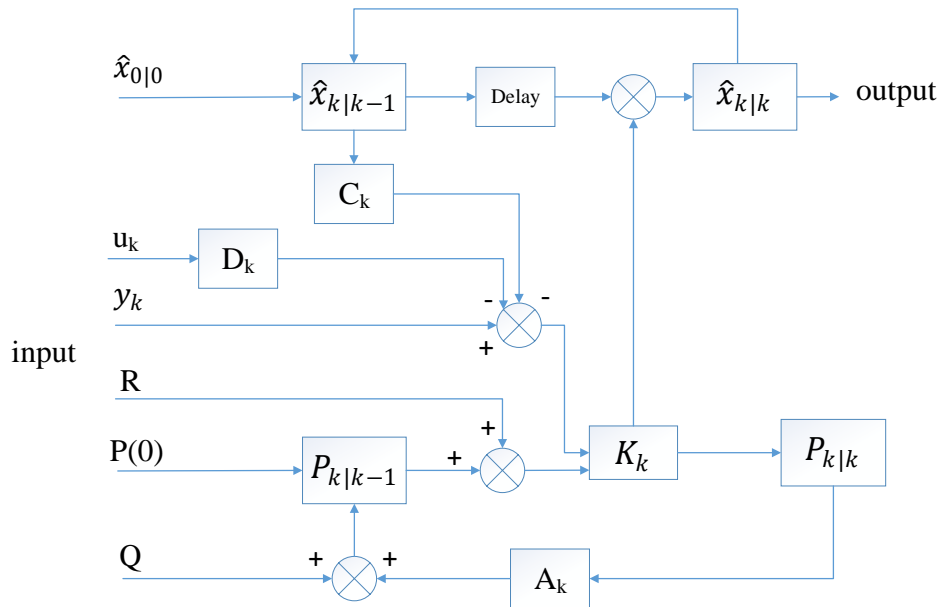

Figure 7. Calculation structure of the LKF.

Notably, the battery system is a highly nonlinear system, and the LKF is only suitable for linear systems. Therefore, two modified KFs, namely, EKF and UKF, were developed in the following two sections for online SOC estimation. Both filters are based on the linear Kalman framework and have a similar prediction–update structure.

4.2. Extended Kalman filter

EKF is an approximation approach that generalizes the LKF to nonlinear systems. The nonlinear state–space equation and measurement discretized equation are given by

$$x_{k+1} = f(x_k, u_k) + \Gamma_k \omega_k \qquad (14)$$
$$y_{k+1} = h(x_k, u_k) + v_k \qquad (15)$$

Same as in the linear Kalman, ω_k and v_k are the zero–mean white Gaussian noise. $f(x_k, u_k)$ is the nonlinear state–function and $h(x_k, u_k)$ is the nonlinear measurement–function.

If $f(.,.)$ and $h(.,.)$ are differentiable functions, then $f(x_k, u_k)$ and $h(x_k, u_k)$ can be linearized by the first-order Taylor–series expansion:

$$f(x_k, u_k) \approx f(\hat{x}_k, u_k) + \frac{\partial f(x_k, u_k)}{\partial x_k}|_{x_k = \hat{x}_k}(x_k - \hat{x}_k) \qquad (16)$$
$$h(x_k, u_k) \approx h(\hat{x}_k, u_k) + \frac{\partial h(x_k, u_k)}{\partial x_k}|_{x_k = \hat{x}_k}(x_k - \hat{x}_k) \qquad (17)$$

Let $\hat{A}_k = \frac{\partial f(x_k, u_k)}{\partial x_k}|_{x_k = \hat{x}_k}$, $\hat{C}_k = \frac{\partial h(x_k, u_k)}{\partial x_k}|_{x_k = \hat{x}_k}$, then the nonlinear functions are transformed to:

$$x_{k+1} \approx \hat{A}_k x_k + [f(\hat{x}_k, u_k) - \hat{A}_k \hat{x}_k] + \Gamma_k \omega_k \qquad (18)$$
$$y_k \approx \hat{C}_k x_k + [h(\hat{x}_k, u_k) - \hat{C}_k \hat{x}_k] + v_k \qquad (19)$$

By the above linear transformation, the EKF is developed and the algorithm steps are similar to the LKF, as shown in equations (7) – (13). To avoid repetition, the details are not reiterated here.

4.3. Unscented Kalman filter

Unscented Kalman is another alternative approach for linearizing the systems with UT transform. The key part and the first step of this algorithm is to set up a set of sigma points. The procedure is described in detail below.

We assume that χ is an n-dimension vector that obeys $X=N(\chi, P)$ distribution.

Initialization:

$$\bar{x}_0 = E(x_0), P_0 = [(x_0 - \bar{x}_0)(x_0 - \bar{x}_0)^T] \qquad (20)$$

Then, the sigma points with their weights are computed as follow:

$$\chi_{i,k-1} = \begin{cases} \bar{x}_{k-1}, & i = 0 \\ \bar{x}_{k-1} + \left(\sqrt{(n+\lambda)P_{k-1}}\right), & i = 1, 2, \dots, n \\ \bar{x}_{k-1} - \left(\sqrt{(n+\lambda)P_{k-1}}\right), & i = n+1, \dots, 2n \end{cases} \qquad (21)$$

$$W_0^m = \frac{\lambda}{(n+\lambda)} \qquad (22)$$

$$W_i^m = \frac{1}{2(n+\lambda)} \qquad i = 1, \dots, 2n \qquad (23)$$

$$W_0^c = \frac{\lambda}{(n+\lambda)} + (1 - \alpha^2 + \beta) \qquad (24)$$

$$W_i^c = \frac{1}{2(n+\lambda)} \qquad i = 1, \dots, 2n \qquad (25)$$

$$\lambda = \alpha^2(n+\kappa) - n \qquad (26)$$

where λ is the scaling parameter, α is a small positive number and κ is either 0 or 3-n. β incorporates the prior information of x.

After the sigma points generated, the UKF algorithm is operated by the following steps:

Prediction update:

$$\chi_{i,k|k-1} = f(\chi_{i,k-1}), \qquad i = 0, \dots, 2n \qquad (27)$$

$$\bar{x}_{k|k-1} = \sum_{i=0}^{2n} W_i^m \chi_{i,k|k-1} \qquad (28)$$

$$P_{k|k-1} = \sum_{i=0}^{2n} W_i^c (\chi_{i,k|k-1} - \bar{x}_{k|k-1})(\chi_{i,k|k-1} - \bar{x}_{k|k-1})^T + Q \qquad (29)$$

where $f(.)$ is the nonlinear state transfer function, and Q is the covariance matrix of the state noise.

Measurement update:

$$y_{i,k|k-1} = h(\chi_{i,k-1}), \qquad i = 0, \dots, 2n \qquad (30)$$

$$\bar{y}_{k|k-1} = \sum_{i=0}^{2n} W_i^m \chi_{i,k-1} \qquad (31)$$

$$P_{yy,k} = \sum_{i=0}^{2n} W_i^c (y_{i,k|k-1} - \bar{y}_{k|k-1})(y_{i,k|k-1} - \bar{y}_{k|k-1})^T + R \qquad (32)$$

$$P_{xy,k} = \sum_{i=0}^{2n} W_i^c (\chi_{i,k|k-1} - \bar{x}_{k|k-1})(y_{i,k|k-1} - \bar{y}_{k|k-1})^T \qquad (33)$$

where $h(.)$ is the nonlinear measurement function, and R is the covariance matrix of the measurement noise.

Kalman gain update:

$$K_k = \frac{P_{xy,k}}{P_{yy,k}} \qquad (34)$$

Correct the posterior value:

$$\bar{x}_{k|k} = \bar{x}_{k|k-1} + K_k(y_k - \bar{y}_{k|k-1}) \qquad (35)$$

$$P_{k|k} = P_{k|k-1} - K_k P_{yy,k} K_k^T \qquad (36)$$

4.4. Implementation for SOC estimation

In this study, the battery model proposed in Section 3.1 is combined with the EKF and UKF algorithms separately. First, the battery model is discretized as

$$\begin{bmatrix} U_{p,k} \\ SOC_k \end{bmatrix} = \begin{bmatrix} 1 - \frac{T_s}{C_p R_p} & 0 \\ 0 & 1 \end{bmatrix} \begin{bmatrix} U_{p,k-1} \\ SOC_{k-1} \end{bmatrix} + \begin{bmatrix} \frac{T_s}{C_p} \\ \frac{\eta_k T_s}{C_N} \end{bmatrix} [I_{k-1}] + \begin{bmatrix} \omega_{1,k-1} \\ \omega_{2,k-1} \end{bmatrix} \qquad (37)$$

$$[U_{l,k}] = [1 \quad 0] \begin{bmatrix} U_{p,k} \\ SOC_k \end{bmatrix} + [R_0][I_{l,k}] + [U_{oc}] + [v_k] \qquad (38)$$

where T_s is the sampling time, C_N is the battery nominal capacity, and η_k is the charge–discharge efficiency.

Then, according to Equation (37) and (38), we define

$$x_k = \begin{bmatrix} U_{p,k} \\ SOC_k \end{bmatrix}, A_k = \begin{bmatrix} 1 - \frac{T_s}{C_p R_p} & 0 \\ 0 & 1 \end{bmatrix}, B_k = \begin{bmatrix} \frac{T_s}{C_p} \\ \frac{\eta_k T_s}{C_N} \end{bmatrix}, C_k = \frac{\partial U_l}{\partial x} = \begin{bmatrix} \frac{\partial U_l}{\partial U_p} & \frac{\partial U_l}{\partial SOC} \end{bmatrix}$$

Finally, we substitute the above expressions into Equation (18) – (19), the SOC is estimated recursively by repeating the procedures described in Sections 4.2 and 4.3. Specifically, T_s is 1 s according to the sampling rate. The tuning parameters are listed in Table 2. For comparability, both filters use the same tuning parameters. The nominal capacity is 2.5 Ah. However, the actual capacity is the function of discharge rate and ambient temperature, which is discussed further in the next section.

Table 2. Tuning parameters setup for the EKF and UKF

| Parameter | Q | R | Sigma point | | |
			α	β	κ
Value	$\begin{bmatrix} 0.01 & 0 \\ 0 & 0.0001 \end{bmatrix}$	0.001	0.02	2	1

4.5. Improvement of the proposed algorithm

In real-world applications, the total capacity can be temporally changed because of the external factors, such as discharge rate and temperature. Here, the model accuracy can be improved by recalibrating the capacity of the cells. Thus, the multiple-rate discharge test described in Section 2.2 was carried out. Six discharge curves were obtained, as shown in Fig. 8 (a). Meanwhile, Fig. 8 (b) shows the discharge rate–temperature–capacity map. In practical conditions, the available capacity is interpolated by the rate–temperature–capacity table.
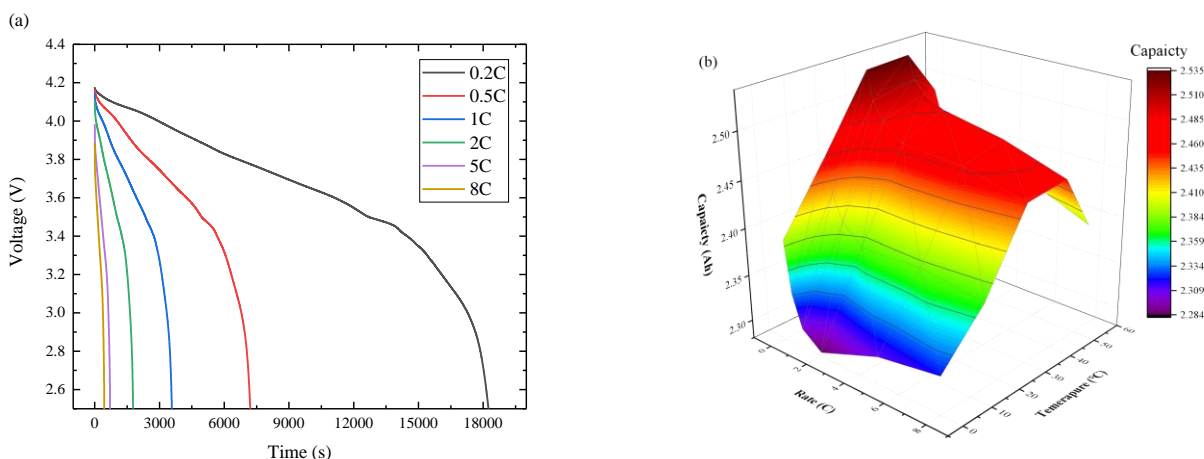
Figure 8 (a) Discharge curves of the cell under different rate, **(b)** Three-dimensional look-up table of the total available capacity.

5. RESULTS AND DISCUSSION

The estimation performance of EKF was compared with that of UKF by employing the validation test in Section 2.4. To make the performance of the two filters more comparable, we uniformly set the tuning parameters of matrix P, process noise matrix Q, and measurement noise R, as shown in Table 2.

Fig. 9 shows the estimated SOC and error of the two filters at different temperatures when the SOC is initialized to the true value of 90%. The results were compared to the true SOC, which was calculated by the battery test station. The max estimation error of EKF was approximately 3%, whereas that of the UKF was approximately 2.5%. The estimated voltage error for our proposed model (see Fig. 6) was larger at low temperatures than that at high temperatures. Consequently, the estimation accuracy deteriorated as the temperature decreased. Especially in EKF, the effect of temperature was substantial. UKF can achieve a higher estimation accuracy than EKF at all temperatures. In other words, the estimation accuracy of EKF is more dependent on the ECM's accuracy. The numerical results of MAE and RMSE of the two filters are presented in Tables 3 and 4, respectively. At 0 °C, the MAE values of the EKF and UKF were 1.536% and 1.354%, respectively, indicating an improvement of 11.8%. The RMSE of the EKF was 1.927%, whereas that of UKF was 1.719%, indicating an improvement of 10.4%. These results indicate that the UKF achieves better accuracy in SOC estimation regardless of temperature.
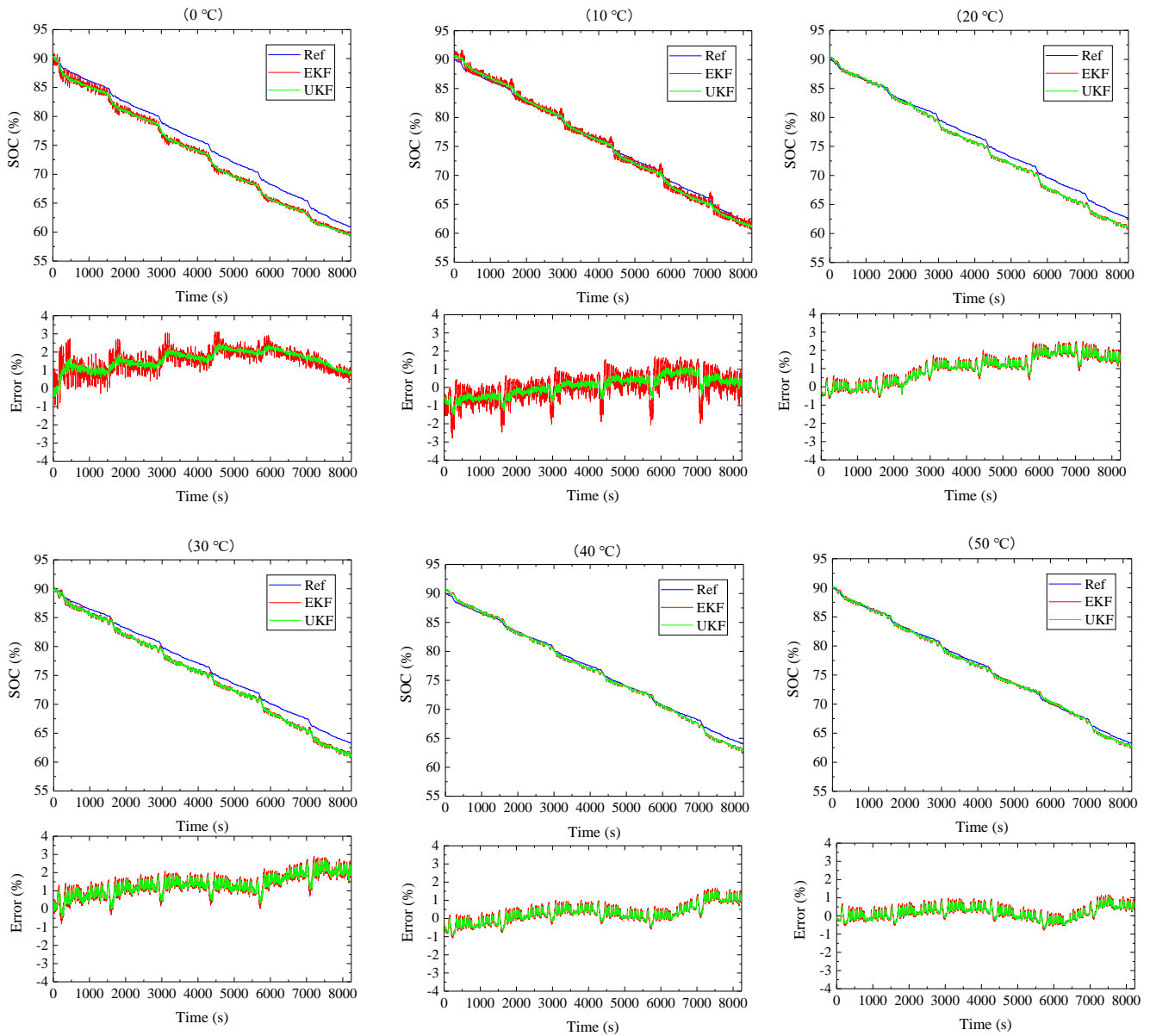
Figure 9. SOC estiamation results and error of the EKF and UKF at different temperatures.

Table 3. The MAE of the two algorithms at different temperatures.

Algorithm	Temperature					
	0 °C	10 °C	20 °C	30 °C	40 °C	50 °C
EKF	1.536	0.581	1.048	1.345	0.445	0.327
UKF	1.354	0.441	1.031	1.337	0.422	0.300

Table 4. RMSE of the two algorithms at different temperatures**.**

Algorithm	Temperature					
	0 ℃	10 ℃	20 ℃	30 ℃	40 ℃	50 ℃
EKF	1.927	0.822	1.236	1.467	0.573	0.405
UKF	1.719	0.725	1.220	1.444	0.542	0.369

The voltage sensor of real-world BMS applications usually have a ±5 V range and a 0.2% sensor accuracy. Therefore, to investigate the robustness of the two filters, we designed a +10 mV voltage measurement offset such that the voltage sensor drift in the BMS is simulated. The simulation was carried out with the profiles at 50 ℃, with the initial guess of the SOC set to 50%. Fig. 10 (a) shows the result of the estimated SOC of the two filters, and Fig. 10 (b) illustrates the estimated error. After the estimated SOC quickly converged to the true SOC, the curves showed a behavior similar to that observed in Fig. 6 (c). Thus, both filters have good robustness against the uncertainty of the initial SOC information and voltage sensor drift. In Refs. [43, 44], a similar comparative work between EKF and UKF was conducted, the estimation accuracy was validated under a specific condition. Here, we extended the validation test to broader application scenarios and achieved a considerable accuracy. To futher demonstrate the pros and cons of our proposed algorithm in SOC estmaiton, the proposed method is compared with other similar technologies which have been published. The results are compared and listed in Table 5.
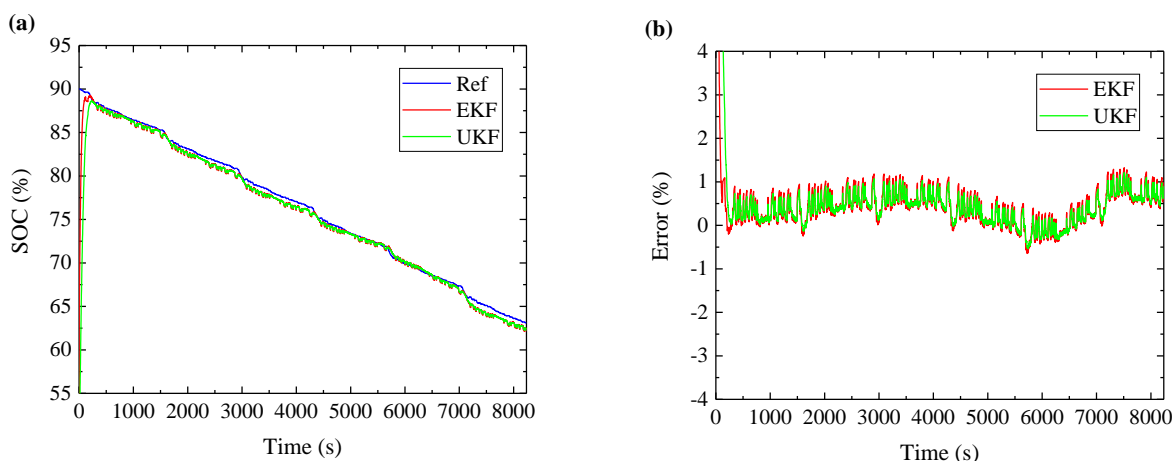

Figure 10. The SOC estimation results and error of EKF and UKF with +10 mV voltage offset and initial SOC of 50% at 50 ℃ .

From the above discussion, we can conclude that UKF outperforms EKF with respect to accuracy and robustness at different ambient temperatures. In Section 3.3, the voltage tracking capability of the improved model was evaluated by comparing it with the conventional model. Here, the two models for SOC estimation was compared by using the UKF. The battery system of an EV or a hybrid vehicle usually experiences a relative high ambient temperature due to the cells' heat production and lack of heat rejection. Thus, we used a 50 ℃ test data to verify our proposed model, as presented in Fig. 11. As

expected, the modified model using UKF improved the the SOC estimation accuracy. The MAE of the SOC error was 0.763% for the original model and 0.310% for the modified model, indicating an improvement of 59.4%. The RMSE of the SOC error was 0.862% for the original model and 0.381% for the modified model, indicating an improvement of 55.8%. The conventional model showed an overestimation behavior. We attempted to explain this result by the available capacity. As shown in Fig. 8 (b), the total available capacity reached a peak value at 30 °C and started to decline. The conventional model lacked correction of the total capacity at different temperatures, resulting in the overestimation of SOC.

Table 5. Accuracy comparion of the proposed algorithm to others.

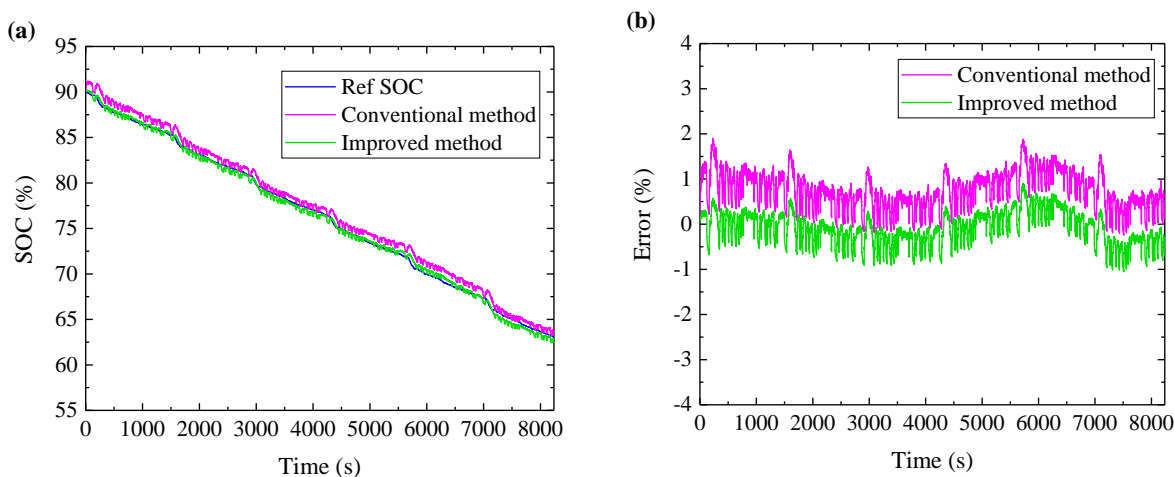| Algorithm	Refs.	Average error
EKF	[45]	≤5%
	[46]	≤5%
	[47]	≤5%
	[48]	≤4%
	[49]	≤5%
UKF	[50]	≤4%
	[22]	≤4%
	[23]	≤4%

Figure 11. SOC estimation results and errors of proposed model and origin model at 50 °C.

4. CONCLUSION

The KF is considered an effective tool for online SOC monitoring. Consequently, the number of studies on different kinds of KFs, especially nonlinear KF, has markedly increased. However, shortcomings remain. First, the estimation accuracy and robustness of KFs is dependent on tuning

parameters. To the authors' best knowledge, few comparative studies about KFs have discussed unified tuning parameters. Second, numerous studies have considered ambient temperature, but the validations of the filter performance have been only carried out at specific temperatures.

In this research, two nonlinear KFs, namely, EKF and UKF, were introduced and compared. To validate the performance of these two filters, we proposed a modified ECM with a temperature module. The proposed battery model was identified by the HPPC at 0 °C, 15 °C, 30 °C, 45 °C, and 55 °C and validated by a self-designed high dynamic current load at 0 °C, 10 °C, 20 °C, 30 °C, 40 °C, and 50 °C, respectively. In general, UKF is superior to EKF.

Our proposed model was compared with the conventional model, which does not consider temperature. The results showed that the maximum voltage tracking ability of our proposed model is better than the conventional model by 50.9%, without overcomplicating the model. Furthermore, the proposed model was applied to the EKF and UKF algorithms for online SOC monitoring. The performace of the two fiters were also validated by our self-designed profile at the temperature of 0 °C, 10 °C, 20 °C, 30 °C, 40 °C, and 50 °C, respectively. The validation coverd from a 60% to 90% SOC range. For the comparative evaluation, the same tuning paramter sets were used. The estimated accuracy of both filters showed a temperature–dependent behavior, although the EKF was more affected. The robustness of the two filters was investigated by setting a +10 mV voltage offset and a 50% initial SOC in the simulation. The UKF exhibited a better performance in terms of convergence behavior and estimation accuracy. The SOC estimation performance of our modified model and the original model were compared through the UKF method. The MAE was improved by 59.4%, whereas the RMSE was improved by 55.8% at 50 °C.

In our future work, the algorithms will be implemented in a rapid control prototyping (RCP) test bench to evaluate the computing effort and monitor the stability. Moreover, the battery health condition will be considered.

References

1. B. Scrosati, J. Garche, *J. Power Sources*, 195 (2010) 2419.
2. C. Zhang, F. Yan, C. Du, J. Kang, R. Turkson, *Energies*, 10 (2017) 110.
3. Y. Wang, C. Zhang, Z. Chen, *Appl. Energy*, 137 (2015) 427.
4. K.S. Ng, C.-S. Moo, Y.-P. Chen, Y.-C. Hsieh, *Appl. Energy*, 86 (2009) 1506.
5. A. Fotouhi, K. Propp, D.J. Auger, *IEEE Comput. Sci. Electronics Eng. Conf.*, (2015) 243.
6. F. Liu, T. Liu, Y. Fu, *IEEE Int. Symp. Comput. Intelligence Des.*, (2015) 152.
7. J.C. Alvarez Anton, P.J. Garcia Nieto, C. Blanco Viejo, J.A. Vilan Vilan, *IEEE Trans. Power Electron.*, 28 (2013) 5919.
8. G.L. Plett, *J. Power Sources*, 134 (2004) 252.

9. G.L. Plett, *J. Power Sources*, 134 (2004) 262.
10. G.L. Plett, *J. Power Sources*, 134 (2004) 277.
11. A.M. Bizeray, S. Zhao, S.R. Duncan, D.A. Howey, *J. Power Sources*, 296 (2015) 400.
12. H. Fang, Y. Wang, Z. Sahinoglu, T. Wada, S. Hara, *Control Eng. Pract.*, 25 (2014) 45.
13. G. Pérez, M. Garmendia, J.F. Reynaud, J. Crego, U. Viscarret, *Appl. Energy*, 155 (2015) 834.
14. S. Sepasi, R. Ghorbani, B.Y. Liaw, *J. Power Sources*, 245 (2014) 337.
15. S. Sepasi, R. Ghorbani, B.Y. Liaw, *J. Power Sources*, 255 (2014) 368.
16. S. Wang, C. Fernandez, L. Shang, Z. Li, J. Li, *J. Energy Storage*, 9 (2017) 69.
17. J. Lee, O. Nam, B.H. Cho, *J. Power Sources*, 174 (2007) 9.
18. E.A. Wan, R.v.d. Menve, *IEEE Trans. Syst. Signal Process. Commun. Control Symp.*, (2000) 153.
19. G.L. Plett, *J. Power Sources* 161, (2006) 1356.
20. G.L. Plett, *J. Power Sources* 161, (2006) 1369.
21. W. He, N. Williard, C. Chen, M. Pecht, *Int. J. Electrical Power Energy Syst.*, 62 (2014) 783.
22. W. He, N. Williard, C. Chen, M. Pecht, *Microelectron. Reliab.*, 53 (2013) 840.
23. Y. Tian, B. Xia, W. Sun, Z. Xu, W. Zheng, *J. Power Sources*, 270 (2014) 619.
24. D. Andre, A. Nuhic, T. Soczka-Guth, D.U. Sauer, *Eng. Appl. Artif. Intell.*, 26 (2013) 951.
25. C. Campestrini, T. Heil, S. Kosch, A. Jossen, *J. Energy Storage*, 8 (2016) 142.
26. X. Hu, S. Li, H. Peng, *J. Power Sources*, 198 (2012) 359.
27. J. Li, J. Klee Barillas, C. Guenther, M.A. Danzer, *J. Power Sources*, 230 (2013) 244.
28. Y. Xing, W. He, M. Pecht, K.L. Tsui, *Appl. Energy*, 113 (2014) 106.
29. F. Yang, Y. Xing, D. Wang, K.-L. Tsui, *Appl. Energy*, 164 (2016) 387.
30. Y. He, X. Liu, C. Zhang, Z. Chen, *Appl. Energy*, 101 (2013) 808.
31. H. G, Usabc Electric Vehicle Battery Test Procedures Manual, 2015.
32. F. Sun, X. Hu, Y. Zou, S. Li, *Energy*, 36 (2011) 3531.
33. X. Han, M. Ouyang, L. Lu, J. Li, *J. Power Sources*, 278 (2015) 814.
34. S. Santhanagopalan, R.E. White, *J. Power Sources*, 161 (2006) 1346.
35. A.P. Schmidt, M. Bitzer, Á.W. Imre, L. Guzzella, *J. Power Sources*, 195 (2010) 7634.
36. Z. Deng, L. Yang, Y. Cai, H. Deng, *Energy Procedia*, 107 (2017) 68.
37. Y. Huang, L. Xu, Q. Luo, X. Kuang, *Appl. Math. inf. Sci.*, 7 (2013) 625.
38. H. Sheng, J. Xiao, *J. Power Sources*, 281 (2015) 131.
39. H. Dai, X. Wei, Z. Sun, J. Wang, W. Gu, *Appl. Energy*, 95 (2012) 227.
40. L. Wang, L. Wang, C. Liao, J. Liu, *IEEE Vehicle Pow. Propul. Conf.*, (2009) 1938.
41. W.B. Gu, C.Y. Wang, *J. Electrochem. Soc.*, 147 (2000) 2910.
42. A. Nyman, T.G. Zavalis, R. Elger, M. Behm, G. Lindbergh, *J. Electrochem. Soc.*, 157 (2010) A1236.
43. M. Shehab El Din, A.A. Hussein, M.F. Abdel-Hafez, *IEEE Trans. Transp. electrif.*, 4 (2018) 408.
44. X. Zhang;, J. Wu;, G. Kang, Int. Confer. *Ubiquitous Robots Ambient Intell.*, (2016) 945.
45. C.Y. Chun, G.-S. Seo, B.-H. Cho, J. Kim, *IEEE ECCE Asia Downunder*, (2013) 912.
46. Z. Chen, Y. Fu, C.C. Mi, *IEEE Trans. Veh. Technol.*, 62 (2013) 1020.
47. J. Kim, G.-S. Seo, C. Chun, B.-H. Cho, S. Lee, *Int. Electr. Veh. Conf.*, (2012).
48. M. Mastali, J. Vazquez-Arenas, R. Fraser, M. Fowler, S. Afshar, M. Stevens, *J. Power Sources*, 239 (2013) 294.
49. S.J. Lee, J.H. Kim, J.M. Lee, B.H. Cho, *Pow. Electr. Specialists Conf.*, (2007) 2799.
50. W. He, N. Williard, C. Chen, M. Pecht, *Prognostics and Syst. Health Manage. Conf.*, (2012).